Morphological and electronic properties of ultrathin crystalline silica epilayers on a Mo(112) substrate

T. Schroeder, J. B. Giorgi,* M. Bäumer, and H.-J. Freund
Fritz-Haber-Institut der Max-Planck-Gesellschaft, Faradayweg 4–6, 14195 Berlin
(Received 7 March 2002; revised manuscript received 13 June 2002; published 25 October 2002)

Ultrathin crystalline silica layers grown on a Mo(112) substrate have been shown to be a useful silica model oxide support in surface science model catalyst studies. As the oxide support material plays an important role in the catalytic process, a multitechnique surface science study is presented to characterize the morphological and electronic properties of the heteroepitaxial system SiO_2/Mo(112). The long-range order of the silica epilayer which grows commensurate with a $c(2\times2)$ surface unit mesh on the Mo(112) substrate is studied by low-energy electron diffraction (LEED). The defect structure of the silica epilayer is characterized in a spot profile analysis (SPA)-LEED study. Antiphase domain boundaries split the silica epilayer into an array of silica crystal grains whose average size and shape is determined. Aiming to prepare flat silica surfaces, the change in the surface roughness with progress in the film preparation is monitored in a combined SPA-LEED and scanning tunneling microscopy (STM) study and seen to influence also the Si-O stretching frequency in the infrared-reflection-absorption spectroscopy spectra. In STM images of the final silica film an average surface roughness of about 1 Å is detected. It is possible to visualize the silica film unit cell periodicity. A combined anger electron spectroscopy and ultraviolet photoelectron spectroscopy valence band study confirms the silica film stoichiometry and the growth of a 4:2 coordinated silica polymorph on the Mo(112) surface. These various surface science studies allow us to propose models for the growth and structure of the silica epilayer on the Mo(112) surface.

DOI: 10.1103/PhysRevB.66.165422 PACS number(s): 68.35.−p, 68.37.Ef, 68.47.Gh, 79.60.−i

I. INTRODUCTION

One surface science approach to study the structure-reactivity relationship of oxide supported metal catalysts consists of growing the oxide support material on a suitable metal substrate in the form of a thin well-ordered oxide film on which the catalytically active metal clusters are deposited.[1–3] Silica (SiO_2) is a widely used oxide support material in heterogeneous catalysis, but the preparation of suitable model silica surfaces in the form of clean and well-ordered silica oxide films on metal supports remained an experimental challenge.

Goodman *et al.* reported the preparation of stoichiometric, but amorphous silica layers which were grown on Mo(110) (Ref. 4) and Mo(100) (Ref. 5) single crystal surfaces. The same group carried out first model catalyst studies by depositing Cu clusters on the system SiO_2/Mo(110).[6] Kohl *et al.* followed this approach in a more recent work by using again the latter system to study silica supported Rh and Rh/VO_x catalysts.[7] In contrast, Mayer *et al.* and Madey *et al.* deposited Ni (Ref. 8) and Pt (Ref. 9) particles, respectively, on amorphous silica layers prepared by thermal oxidation of Si wafers.

However, the amorphous nature of these model silica surfaces renders a control over the structural aspects of the model catalyst system very difficult. Therefore, these approaches are only of limited use to elucidate in surface science model catalyst studies the structure-reactivity relationship of silica supported metal catalysts. In order to achieve this goal, it is advantageous to use as silica model oxide support a thin crystalline (instead of an amorphous) silica layer on top of a metal substrate. The first successful preparation of such a thin crystalline silica film grown on a Mo(112) single crystal surface has been reported by our group.[10–12] In this way, surface science model catalyst studies of silica supported metal catalyst with structural control have become feasible and first results are available for the system Pd/SiO_2/Mo(112).[13]

As the oxide support is known to play an important role in the catalytic reaction, a multitechnique surface science study is presented in this paper to characterize in detail the properties of the heteroepitaxial system SiO_2/Mo(112). The organization of the paper is as follows. After the introduction in Sec. I, the UHV equipment as well as the preparation recipe to grow well-ordered silica films on a Mo(112) surface is briefly discussed in Sec. II. Section III presents the experimental results of the surface science studies. These results are discussed in Sec. IV and used to set up growth and structure models of the silica epilayer on the Mo(112) surface. Section V gives a summary and an outlook on future work.

II. EXPERIMENTAL

Most of the experiments have been carried out in an Omicron multichamber UHV system with a base pressure of 2×10^{-10} mbar, described in detail elsewhere.[14] A self-designed high-temperature cell (HTC) has been integrated to allow sample manipulation up to 2500 K. The high temperature treatment is required to clean the Mo(112) surface. The cleaning procedure consists of an oxidation step at 1500 K, followed by several high temperature flashes to approximately 2300 K to free the surface from any residual molybdenum oxides.[14] Reference spectra, taken immediately after crystal cleaning, are labeled with the number (0).

The silica film preparation usually starts with four cycles

of silica deposition which are labeled by the numbers 1 to 4. For reasons given below, one study required the preparation of a thicker film than usual so that two additional silica deposition cycles denoted 4^{+} and 4^{++} have been applied. Each of these silica deposition cycles consists of a Si deposition step followed by an oxidation step. During the Si deposition, a focus EFM 3 evaporator, calibrated with the help of a quartz microbalance, is used to evaporate by electron bombardment of a silicon rod approximately half a monolayer of Si on the Mo(112) crystal which is kept at 300 K. The subsequent oxidation is carried out at 800 K in an atmosphere of about 5×10^{-6} mbar O_2 for 6 min. After the deposition of the silica film is completed, four annealing steps are applied which take 15 min each in an oxygen background of 1×10^{-5} mbar. The temperature is gradually increased by about 50 K by progressing from one annealing step to the next and usually ranges from 1100 to 1250 K. Spectra taken during SiO_2 film annealing are denoted by the numbers 5 to 8 according to the respective annealing step.

Sample transfer is carried out under UHV conditions for further sample characterization. The main chamber is equipped with a four-grid LEED optics and a hemispherical electron energy analyzer (SES 200) for sample characterization by low-energy electron diffraction (LEED), auger electron spectroscopy (AES), and x-ray/ultraviolet photoelectron spectroscopy (XPS/UPS) studies, respectively. All UP spectra reported in this work have been recorded at normal emission and the photoelectron peak positions are referenced with respect to the Mo(112) Fermi level (zero point of the energy scale). An Omicron VT-STM (variable temperature scanning tunneling microscope) has been used for real space studies of the surface in the constant current mode at room temperature. Finally, a Bruker IFS 66*v*/*S* IR spectrometer is attached to an IR cell of the chamber to carry out *i*nfrared-*r*eflection-*a*bsorption *s*pectroscopy (IRAS) studies in the spectral range from 650 to 4000 cm^{-1}, using *p*-polarized IR light under grazing incidence ($\Phi=84°$). In addition, spot profile analysis LEED studies with a SPA-LEED optics (Leybold) have been carried out in a different chamber.

III. EXPERIMENTAL RESULTS

A. Crystallinity and defects

After introducing the surface crystallography of the Mo(112) substrate surface, LEED, SPA-LEED, STM, and IRAS studies are presented to characterize the morphological properties of the heteroepitaxial system SiO_2/Mo(112).

1. The long range order of the silica epilayer

Figure 1 shows a perspective view of the clean Mo(112) substrate surface. The (112) surface of a bcc crystal consists of close-packed atomic rows orientated along the $\vec{a}_1=[\bar{1}\bar{1}1]$ direction which are separated by furrows in the $\vec{a}_2=[\bar{1}10]$ direction. A rectangular surface unit mesh results with a unit cell spacing of 2.73 and 4.45 Å along the $[\bar{1}\bar{1}1]$ and the $[\bar{1}10]$ directions, respectively. According to its unit mesh in real space, the Mo(112) surface shows a rectangular LEED pattern. In the nomenclature applied in the following,

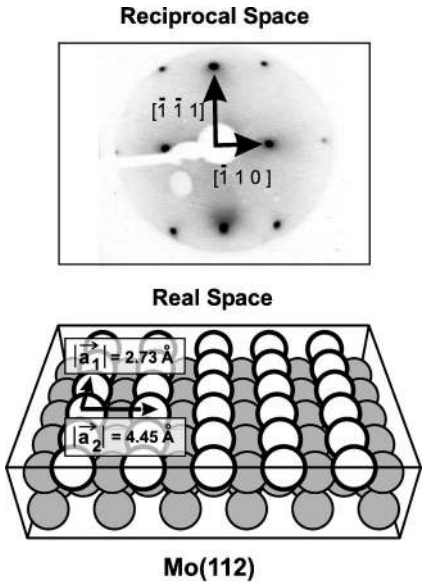

FIG. 1. LEED pattern ($E=56$ eV) and perspective view of the trough and row structure of the Mo(112) surface. The rectangular surface unit mesh is indicated in the reciprocal as well as in the real space image.

spots at the positions of the former substrate spots are referred to as fundamental spots. STM topographs of the clean Mo(112) surface have been recently published by our group in a combined LEED/STM study of an oxygen-induced $p(2\times3)$ surface reconstruction of the Mo(112) surface.[15]

Inverted LEED images ($E=56$ eV) of the silica layer on the Mo(112) surface are shown in Fig. 2. Superlattice spots

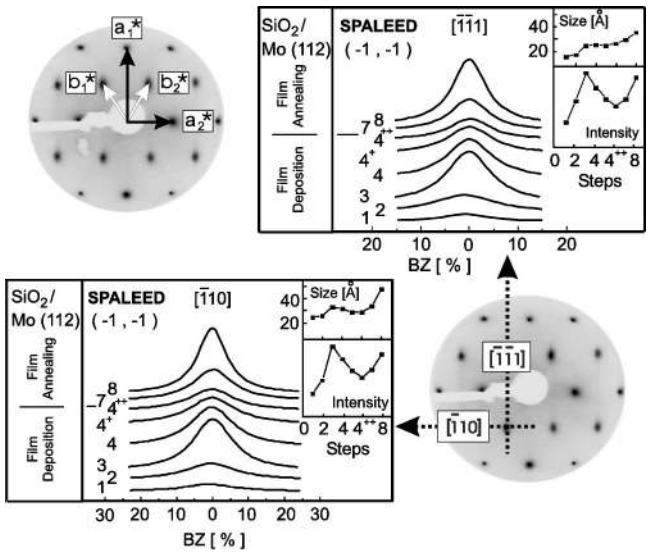

FIG. 2. SPA-LEED data ($E=56$ eV) of the $(-1,-1)$ superlattice spot profiles along the $[\bar{1}\bar{1}1]$ and the $[\bar{1}10]$ direction during the silica film deposition ($1-4^{++}$) and during the silica film annealing procedure (7 and 8). Along each of these substrate directions, the size of the crystalline silica domains (upper insets) and the integrated profile intensity (lower insets) have been derived during the silica film preparation.

of similar intensity as the fundamental spots are now present in the center of the substrate unit meshes. The film unit mesh $\vec{b}^*$ can be described as a $c(2\times2)$ overstructure with respect to the substrate unit mesh $\vec{a}^*$, indicating a pseudomorphic growth of the silica layer on the Mo(112) surface. Using the known dimensions of the substrate unit mesh as an internal standard in the LEED pattern, the real space unit cell dimension of the commensurate silica film unit mesh $\vec{b}$ is derived to be 5.22 Å. Due to the axis ratio of the substrate unit mesh, the film unit cell vectors $\vec{b}$ span an angle of 63° so that the symmetry of a $c(2\times2)$ overstructure on the Mo(112) surface is very close to a hexagonal overlayer structure.

2. The defect structure of the silica epilayer

Undercoordinated atoms at defects often show an enhanced reactivity compared to regular sites. To understand in future studies the growth process of deposited metal clusters on the SiO_2 overlayer as well as the interplay of the catalyst and the oxide support in catalytic reactions, an analysis of the defect structure of the silica layer is given here.

(a) Antiphase Domain Boundaries. The LEED patterns of the silica overlayer in Fig. 2 provide some valuable information about the surface defect structure. Moving along the $\vec{a}_1^*=[\bar{1}\bar{1}1]$ direction from the central (0,0) beam, all fundamental spots are sharp and isotropic, but the superlattice spots exhibit a streaky spot shape. This is due to a strong broadening of the superlattice spots primarily along the $[\bar{1}\bar{1}1]$ direction. Along the $\vec{a}_2^*=[\bar{1}10]$ direction, the superlattice spots are also, but only slightly broader than the fundamental spots. Such periodic LEED patterns of sharp and streaky LEED spots have been shown in the literature to arise whenever the long-range order of the surface structure is disturbed by the presence of antiphase domain boundaries.[16]

Two pieces of information can be extracted from this LEED pattern. First, the *orientation of the domain boundaries in real space* determines which spots are broadened in reciprocal space by the presence of these line defects. The extent to which this spot broadening occurs along a given direction in reciprocal space is a direct measure of the line defect density along the same direction in real space. In the present case it is seen that only superlattice spots are broadened along both substrate directions by these lateral surface imperfections and that the broadening is anisotropic and results in an elongated spot shape along the $\vec{a}_1^*=[\bar{1}\bar{1}1]$ direction. Therefore, it can be concluded that the silica epilayer is split in real space by an array of line defects along the $[\bar{1}\bar{1}1]$ and $[\bar{1}10]$ substrate directions. Furthermore, the elongated superlattice spot shape along the $\vec{a}_1^*=[\bar{1}\bar{1}1]$ direction clearly shows that the line defect density is higher along this direction. Secondly, the *average size of the crystalline silica domains* along each of these two substrate directions can be derived from the measured width of the corresponding superlattice spot profiles. For this purpose, a SPA-LEED study is reported in Fig. 2, where the evolution of the profiles of the $(-1,-1)$ superlattice spot during the silica film deposition $(1-4^{++})$ and the silica film annealing procedure (5–8) has been monitored along the $[\bar{1}\bar{1}1]$ and $[\bar{1}10]$ substrate direction (LEED images corresponding to each of these preparation steps have been discussed in a previous publication).[11]

The $(-1,-1)$ spot profiles along both directions are well described by Lorenzian line shapes. The intensity profile of spots affected by the presence of antiphase domain boundaries is given by such a Lorenz function when the statistical size distribution of the domains can be described by a mathematical model of noninteracting film domains with a constant decay probability of the film domain size S.[16] Applying this model of noninteracting film domains to fit the reported line profiles of Fig. 2 allows one to calculate the average size S of the crystalline silica domains along the two substrate directions.[14] The results are shown in the upper insets of Fig. 2. In both directions, the average domain size S reaches a constant value after completing the third deposition cycle for the rest of the silica film deposition procedure ($S_{\bar{1}\bar{1}1}^{-}\approx25$ Å and $S_{\bar{1}10}^{-}\approx30$ Å). It is only during the film annealing process that a marked decrease in the width of the superlattice spot and, in consequence, a strong increase of the domain sizes of the silica film is detected ($S_{\bar{1}\bar{1}1}^{-}\approx35$ Å and $S_{\bar{1}10}^{-}\approx48$ Å).

The lower insets in Fig. 2 show the evolution of the $(-1,-1)$ superlattice spot intensity during the silica film preparation (1–8). An interesting point is the fact that the intensity of the superlattice spot passes a maximum after the third cycle during the silica film deposition procedure $(1-4^{++})$. This can be understood by taking into account that, due to the difficulty to separate the background intensity of the diffraction experiment from the very slowly decaying shoulder structure of the Lorenz profile, the integration limits to derive the intensity have been restricted to the central part of the superlattice spot. As outlined in Sec. II B, the onset of a roughening of the silica surface can then be detected by such a decrease of the integrated intensity whenever the selected beam energy differs from the in-phase scattering condition between the different height levels present on the silica surface. This detected roughening of the silica surface after the formation of a first well-ordered, substrate stabilized silica layer (1–3) continues with progress in the film deposition: growing a thicker silica film than usual by applying to additional depositon steps (4^{+} and 4^{++}) deteriorates the integrated superlattice beam intensity (and the contrast of the LEED pattern) even further. It is only by the interruption of the silica deposition and the application of the film annealing procedure (5–8) that the integrated superlattice beam intensity is recovered and a flat and well-ordered silica surface can be prepared, as further explained in the next section.

(b) Steps. A kinematical SPA-LEED step analysis can be carried out when the surface is rough, but well ordered (top panel of Fig. 3).[17] As LEED patterns of high quality can only be obtained from the silica layer on the Mo(112) surface when the annealing temperature is beyond 1150 K, the step structure on the silica surface has been studied by SPA-LEED after annealing to 1200 K (7) and 1250 K (8). These studies analyze the energy dependence of the angular profile of the (0,0) beam diffracted from the silica surface. As sketched in the top panel of Fig. 3 for two different scattering energies E_1 and E_2, the intensity profile of the (0,0) beam obtained after diffraction from a rough crystalline surface

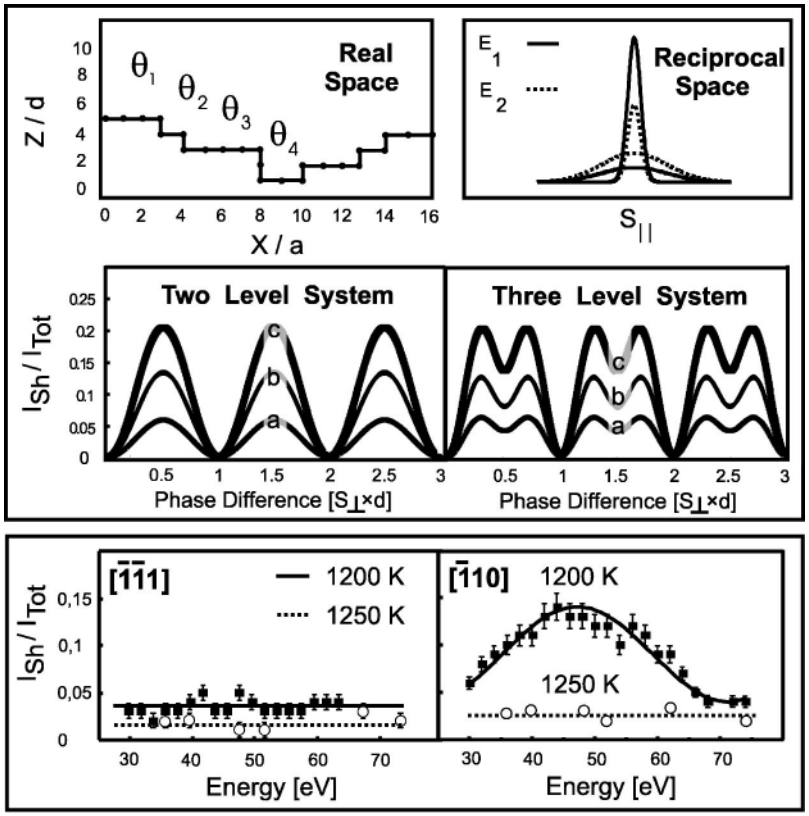

FIG. 3. *Upper panel: (above)* Well-ordered real space surface structure with a lateral spacing a and four different participating surface layers of coverage Θ which set up single and double layer steps of height d and $2d$, respectively (left). Diffraction on a stepped surface at in- and out-of phase conditions conserves the total scattering intensity, but its distribution oscillates in dependence of the diffraction energy between a central spike and the shoulder of the beam (right). (*Below*) Calculated energy dependence of the intensity ratio between shoulder and total intensity for a two (three) level system for various amounts of surface roughnesses [curve a: $\theta_1=0(0.01)$, $\theta_2=0.02(0.01)$, $\theta_3=0.98(0.98)$; curve b: $\theta_1=0(0.02)$, $\theta_2=0.04(0.02)$, $\theta_3=0.96(0.96)$; curve c: $\theta_1=0(0.03)$, $\theta_2=0.06(0.03)$, $\theta_3=0.94(0.94)$]. *Bottom panel*: Step analysis of the SiO_2 overlayer on the Mo(112) surface. The energy dependence of the ratio between shoulder and total diffracted intensity is plotted for the intensity profile of the (0,0) beam along both substrate directions [solid line: annealing step (7) (1200 K); dashed line: annealing step (8) (1250 K)].

consists of a sharp central spike (dominated by the instrument response function of the SPA-LEED optics) and shoulders (determined by the Fourier transform of the generally unknown step distribution function on the surface).[18,19] Their relative intensities depend on the phase relationship for scattering between adjacent levels, i.e., the energy. Changing from an in-phase to an out-of phase energy, a decrease in the sharp central spike region and an intensity increase in the shoulder structure is observed (and vice versa). In consequence, the ratio between the shoulder and the total scattering intensity of the (0,0) beam oscillates as a function of the scattering energy. The simulations in Fig. 3 show this behavior for a two- and a three-level system (see specifications of the surface roughness in the figure caption). In-and out-of phase conditions are seen to result in minima and maxima in these plots, respectively. These simulated curves can be compared with the experimental data of the silica film on the Mo(112) surface (bottom panel of Fig. 3).

After annealing the silica film to about 1200 K, no energy dependent oscillation of the ratio between the detected Gaussian shoulder and the total scattering intensity of the (0,0) beam can be measured along the $[\bar{1}\bar{1}1]$ direction, but it is clearly evolved along the $[\bar{1}10]$ direction. Due to the absence of side minima in the experimental curve, it is concluded that a two-level system is sufficient to describe the step structure on the silica surface. The surface coverages of the two-level system can be extracted from the amplitude of the oscillation and the analysis shows a surface level occupation of ~ 5 and $\sim 95\,\%$ for the first and second levels, using the level enumeration of Fig. 3. The step height d between these two levels is calculated from the two subsequent in-phase conditions (minima) in the curve and an average value of $d \sim 2$ Å is derived. It is surprising that the two-level step structure is detected along the $[\bar{1}10]$, but not along the $[\bar{1}\bar{1}1]$ direction. A possible explanation is a step structure on the silica surface in form of terraces whose dimensions are comparable to the transfer width of the SPA-LEED instrument in the $[\bar{1}\bar{1}1]$ direction, but much smaller along the $[\bar{1}10]$ direction.

Applying a further annealing step at 1250 K shows that this step structure on the silica surface is not stable. This is indicated in the SPA-LEED study in Fig. 3 by (a) the further decrease of the ratio between the shoulder and the total intensity along both directions and by (b) the fact that this intensity ratio does not show an energy dependence along the $[\bar{1}10]$ direction anymore. Thus, these SPA-LEED results give strong evidence for the successful preparation of a flat silica surface.

In order to obtain further information, the results of the diffraction study were supplemented by local imaging of the silica surface with STM. All STM topographs have been recorded at room temperature and at high positive sample bias. No change in the surface morphology has been observed by changing the tip bias from $U_T=-3$ to -6 V. Therefore, it is likely that tunneling from the STM tip into the conduction band of the oxide film becomes the dominant tunneling channel in this bias region so that the surface morphology of the silica oxide film is imaged. STM studies of ultrathin silica films on Si wafers reported very similar bias conditions to image the silica oxide layer.[20,21] In addition, it has been found in this study that a sample bias higher than $+6$ V

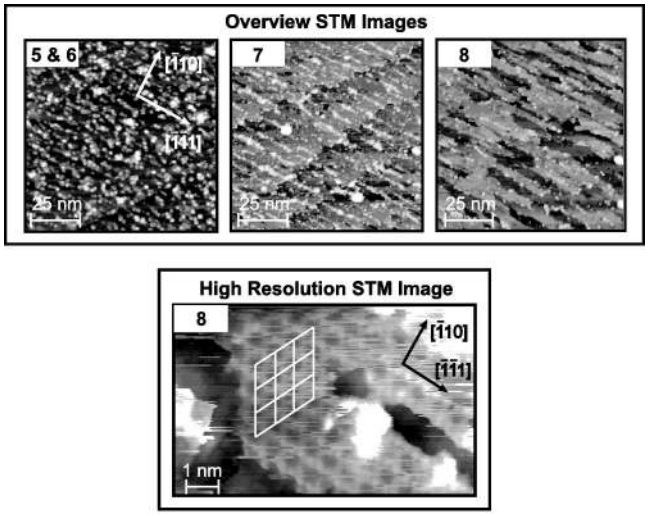

FIG. 4. *Top panel*: Overview STM images (100×100 nm^2; $U_T=-5.8$ V, $I=0.5$ nA [(5 and 6) and (7)]; $U_T=-4.9$ V, $I=0.5$ nA (8)) of the silica surface during the silica film annealing procedure (5–8). The surface morphology changes drastically from a rough, almost granular structure (5 and 6) towards a two-dimensional network of irregular flat terraces (8). An intermediate case is the formation of a step structure in form of stripes with a [$\bar{1}\bar{1}$1] orientation on the silica surface (7). *Bottom panel*: High resolution STM image (5×8 nm^2; $U_T=-0.5$ V, $I=0.5$ nA) of a flat silica terrace from the STM topograph (8). The crystal orientation is the same for all images and is indicated by the coordinate systems.

results in a clear loss of contrast in the images. This and the fact that the STM study failed to achieve atomic resolution is ascribed to the poor conductivity of the wide band gap material silica. Space charge regions are formed in the oxide during the STM experiment at the high bias voltages which tend to smear out the details of the electronic structure of the sample.[22]

Figure 4 shows the results of the STM study of the silica film on the Mo(112) substrate during the silica film annealing procedure (5–8). The first two annealing steps [1100 K (5) and 1150 K (6)] do not change the surface morphology of the freshly deposited silica film. The STM topograph (5 and 6) is a representative real space image of the surface at these film preparation steps. The silica surface is rough and covered with three-dimensional silica conglomerates which coalesce in part and exhibit an average diameter of about 30 Å. As this granular surface structure renders the identification of silica islands with a diameter smaller than 20 Å difficult, only islands of bigger size are used in the following to determine the coverage of the silica surface by silica adislands. Thus, a lower limit of the adisland coverage is given which amounts to approximately 30% of the surface at the end of the annealing steps (5) and (6). The average height of these islands is $\langle 4.8\rangle$ Å. The *root mean* square (r.m.s.) definition of the surface roughness[23] yields a value of approximately 3 Å for the STM topograph (5 and 6). The detection of a rough silica surface by STM at the end of the silica film deposition and during the early annealing steps is in line with the results of the SPA-LEED study (see above).

The following annealing step (7) at 1200 K results in a strong increase of the contrast in the LEED pattern, as can be inferred from the upper insets of Fig. 2 where the superlattice spot intensity is seen to increase at this preparation step. In consequence, a substantial change in the surface topology is expected and indeed detected in the STM study. The STM topograph (7) shows that the surface roughness decreases strongly and a r.m.s. value of just 2 Å is derived. The most characteristic feature of the STM topograph (7) is a step structure in form of bright stripes running along the [$\bar{1}\bar{1}$1] substrate direction. This stripe structure probably results from a decoration of the misfit dislocation lines with [$\bar{1}\bar{1}$1] orientation by silica islands.[14] This idea is supported by the proposed structure models of the silica epilayer discussed in Sec. IV where only the most frequent line defects with [$\bar{1}$10], but not those with [$\bar{1}\bar{1}$1] orientation are seen to be compatible with the silica lattice. Accordingly, a high degree of disorder can be expected for the latter ones so that it is very likely that they serve as nucleation sites for silica adislands. In contrast to the more frequent line defects along the [$\bar{1}$10] direction, this decoration structure allows to image the line defects with [$\bar{1}\bar{1}$1] orientation. The resulting stripe structure shows an average distance of $\langle 40\rangle$ Å in the [$\bar{1}$10] azimuth which is in nice agreement with the above discussed SPA-LEED results for the width of the silica domains in that direction. In addition, a smaller amount of silica adislands are found on the terraces which do not contribute to the formation of the stripes. Counting again only silica adislands with a diameter bigger than 20 Å, it is found that about 8% of the surface is covered by silica conglomerates exhibiting an average height of about 4 ± 1 Å. It is noteworthy that, except for the exact step height, the surface morphology detected by STM (surface coverage and stripe structure along the [$\bar{1}\bar{1}$1] direction) fits well to the results of the corresponding SPA-LEED step analysis [solid lines (1200 K) of annealing step (7) in Fig. 3].

The SPA-LEED step analysis also shows that this stripe structure decays during the last annealing step (8) [dashed curves (1250 K) in Fig. 3]. The STM image (8) shows that indeed a further strong rearrangement of the surface morphology of the silica epilayer has taken place. The r.m.s. value of the surface roughness decreases further to about 1.5 Å. The surface of the final silica epilayer can be described by the presence of an irregular network structure of connected two-dimensional terraces. These terraces have in most cases an elongated shape along the [$\bar{1}\bar{1}$1] direction. Small silica adislands are randomly distributed over these terraces which exhibit on average a height of about 2 Å and a diameter of approximately 20 Å. Adislands of this or a bigger diameter cover about 2% of the surface. Three different terrace levels are identified in the STM images which are separated by an average step height of about $\langle 1\rangle$ Å. This very small step height is probably responsible for the failure of the SPA-LEED study to reflect within the accessible energy range the silica surface morphology after the application of the last annealing step (8).

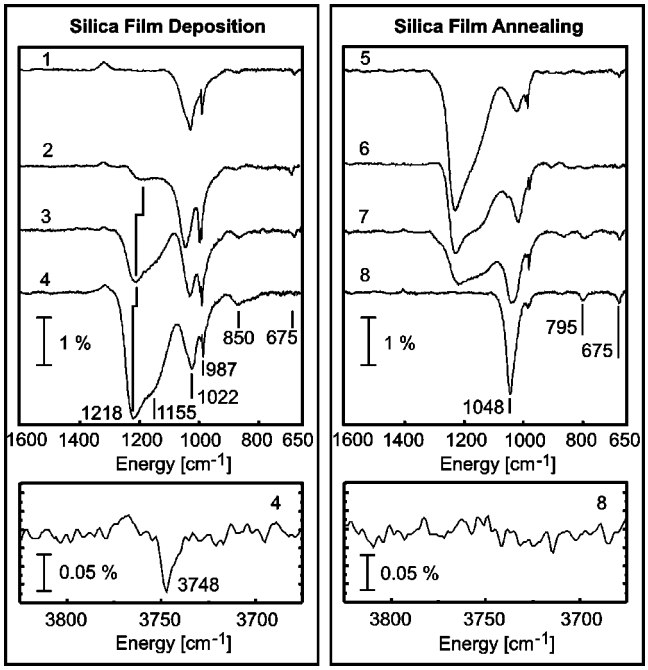

FIG. 5. IRAS spectra of the silica epilayer on the Mo(112) surface during the deposition (1–4) and the annealing (5–8) steps. The upper (bottom) panels show the spectral region from 650 to 1600 cm^{-1} (3600 to 3900 cm^{-1}) (see text).

Figure 4 shows in the bottom panel a high resolution STM image of one of these silica terraces. The STM topograph has been recorded at low tunneling voltages where the tip is in close vicinity to the surface.[24,25] With a detected surface corrugation of about 0.5 Å, the STM study succeeds to image the silica unit cell periodicity. In analogy to the LEED study, white lines sketch these unit cells in form of a $c(2\times2)$ pattern with respect to the Mo(112) surface. A unit cell lattice spacing of about 5 ± 0.5 Å is derived from the STM measurement which is in reasonable agreement with the more accurate value of 5.22 Å reported in the LEED study.

3. The vibrational excitations of the system $SiO_2/Mo(112)$

It has been shown that *P*-polarized IR radiation at oblique incidence can only excite polar optical modes at longitudinal optical frequencies ω_{LO} in an oxide/metal structure.[26,27] The phenomenon that the equivalent of longitudinal optical modes in an infinite medium can be stimulated in thin films by *P*-polarized IR radiation under oblique incidence is known as the Berreman effect.[28]

Figure 5 summarizes the IRAS spectra of the system $SiO_2/Mo(112)$ in the spectral range from 650 to 1600 cm^{-1} (top panels) and 3600 to 3900 cm^{-1} (bottom panels) which have been collected at 300 K during the film deposition [left panel (1–4)] and the annealing process [right panel (5–8)].

The IRAS spectra collected during the *silica film deposition* (1–4) show only very weak IR signals in the wave number region below 900 cm^{-1}. As outlined below and in accordance with recent results of an HREELS study on the oxygen adsorption states on the Mo(112) surface,[29] the small peak structure at 675 cm^{-1} can possibly be assigned to the Mo-O mode of oxygen atoms which are located at the $SiO_2/Mo(112)$ interface in the quasithreefold hollow sites on the Mo(112) surface. The symmetric Si-O stretching modes of moderate IR activity are detected in form of the small bands around 850 cm^{-1}. The IR activity of the symmetric Si-O modes is lower than for the asymmetric Si-O stretching motions in the wave number range from 950 to 1250 cm^{-1} by a factor of 15.[30,31] During the early stage of the silica film deposition (1,2) the IRAS spectra are characterized in this spectral range by a very narrow peak at 987 cm^{-1} [full width at half maximum (FWHM) ~15 cm^{-1}] and a broad band at 1022 cm^{-1} (FWHM ~60 cm^{-1}). The position of the peak at 987 cm^{-1} is very close to the literature value of the Si-O vibration frequency in silanol Si-OH groups (~980 cm^{-1}).[32] The assignment of this peak structure to silanol groups is supported by the small band at 3748 cm^{-1} which corresponds to the O-H frequency in SiO-H groups.[32] All spectra (1–4) show this peak, but only the spectrum (4) at the end of the silica film deposition is shown in the bottom left panel. The broad band at 1022 cm^{-1} is located in the low-frequency limit of the spectral range of the asymmetric Si-O stretching motions.[33–36] It is attributed to the formation of the pseudomorphic initial SiO_2 layer on the Mo(112) surface because it correlates with the appearance of the LEED pattern of good quality during the early stage of the silica deposition. Furthermore, the assignment of this phonon band to an asymmetric Si-O mode which is influenced by the formation of Si-O-Mo species at the interface is supported by IR studies of silica supported molybdenum oxide catalysts.[37] When the molybdenum oxide catalysts are dispersed on the silica support by wet impregnation techniques, these IR studies report (depending on the oxidation state of the molybdenum oxides) the appearance of new asymmetric Si-O absorption bands in the spectral range from 925 to 1110 cm^{-1}. The application of the third and the fourth silica deposition cycle strongly increases the intensity of the small high frequency shoulder at about 1190 cm^{-1} from cycle (2) and shifts the band position to 1208 cm^{-1} (3) and 1218 cm^{-1} (4), respectively. This blueshift in the band position of a silica film vibration can possibly be attributed to a decrease in the coupling strength between the vibrational dipole of the film mode and its own image dipole in the metal substrate when the film grows thicker.[38] Furthermore, a low-frequency shoulder at ~1155 cm^{-1} becomes clearly detectable in this peak after the third (3) and the fourth (4) silica deposition cycle. Both peaks show a FWHM value of approximately 80 cm^{-1} at the end of the silica film deposition (4) and the peak positions allow to identify these IR bands as asymmetric Si-O stretching motions.[39,40] It is interesting to note that the appearance of this double peak structure correlates with the increase of the surface roughness of the silica layer discussed above in the SPA-LEED study for the late silica deposition steps. Therefore, the asymmetric Si-O stretching frequency is clearly seen in this IRAS study to be sensitive to the details of the silica surface morphology. This supports the results of theoretical studies where the surface roughness has been found to strongly influence the positions of the asymmetric LO Si-O modes in thin silica layers.[41]

The idea of the influence of the surface morphology on the asymmetric LO Si-O mode positions is also reflected by the behavior of this double peak structure in the IRAS spectra during the *silica film ánnealing* procedure [spectra (5–8) in the right panel of Fig. 5]. The decrease of the surface roughness of the silica film during the annealing process results in a strong intensity decrease (5–7) and a complete loss (8) of the asymmetric LO Si-O stretching bands at ~1155 and ~1218 cm^{-1}. In contrast to this, the IR band at 1022 cm^{-1} (4) shows an intensity increase and a blue shift to 1048 cm^{-1} (8) during the annealing process. The final flat pseudomorphic silica epilayer on the Mo(112) surface is characterized in the asymmetric Si-O stretching region by this single narrow IR band at 1048 cm^{-1} with a low FWHM value of ~40 cm^{-1}, emphasizing the high degree of the long-range order in the crystalline silica film. It is noteworthy that the high temperature treatment also widely removes the silanol groups in the system SiO_2/Mo(112). This can be concluded from the IRAS spectrum of the final silica layer (8) where the IR bands at 987 cm^{-1} (right top panel) and 3748 cm^{-1} (right bottom panel) are almost absent.

Furthermore, it is an important result that the spectrum (8) of the final silica film proves the absence of a phonon band at 723 cm^{-1}. As this IR peak indicates the formation of molybdenum oxides,[42] this experimental finding gives strong evidence for the formation of a closed silica layer which passivates the Mo(112) surface against oxidation during the annealing procedure. This supports the results of previous studies where the continuous nature of the silica layer on the Mo(112) substrate has been proven by TDS and XPS studies.[11,12]

B. Stoichiometry and valence bands

In previous publications, XPS studies have proven the stoichiometric nature of the silica epilayers on the Mo(112) surface.[11,12] In particular, the study confirmed the absence of silicon and molybdenum suboxides as well as molybdenum silicides in the system SiO_2/Mo(112). A further important result for the construction of the structure models of the silica epilayer on the Mo(112) surface in Sec. IV is the detection of an oxygen species of the type Si-O-Mo in the XPS O_{1s} spectra which, located at the interface, was proposed to connect the silica film lattice to the Mo(112) substrate surface. These data are now supplemented by AES and UPS studies which provide detailed insights in the valence band structure.

Figure 6 shows in the left panel the results of the Auger electron spectroscopy study. The upper spectrum of the clean Mo(112) surface (0) exhibits a multiple peak structure which is due to different *MNN*, *MNV*, and *MVV* transitions.[43] Here, the only peak of interest is the most intense $M_{4,5}NV$ transition at 187 eV. The attenuation of this peak after the deposition of the silica film [spectrum (8)] was used to determine the silica film thickness. A value of 7 ± 2 Å was derived which was also confirmed by an ARXPS measurement.[14] The Auger spectrum of freshly deposited Si (0.5) is marked by the Si $L_{2,3}VV$ Auger transition of elemental Si at 92 eV.[44] A simultaneously detected small peak at 83

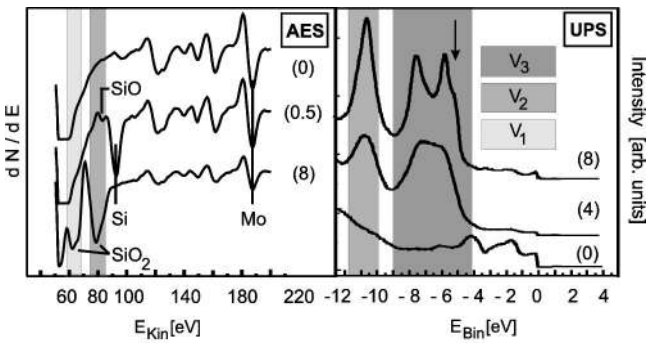

FIG. 6. *Left panel*: Differentiated AE spectra of the clean Mo(112) surface (0), clean Si on Mo(112) (0.5), and the silica film on the Mo(112) substrate (8). *Right panel*: He I UPS valence band study of the clean Mo(112) surface (0), the freshly deposited silica film (4) and the final silica epilayer on the Mo(112) surface (8). The gray panels V_1, V_2, and V_3 depict the contributions of the three well-known silica valence band regions to the spectra (see text).

eV is close to the value of the Si $L_{2,3}VV$ transition for SiO (84 eV) and marks the initial change in the silicon valence band due to oxidation.[45] This unavoidable partial oxidation of the freshly deposited Si on the clean Mo(112) surface at room temperature can probably be attributed to the well-known silicon low temperature reactivity in the vicinity of metal interfaces.[46] The last AE spectrum (8) is collected from the final silica film on the Mo(112) surface. In line with reference spectra taken from bulk 4:2 coordinated silica samples, the Si $L_{2,3}VV$ line shape of the silica epilayer is now split into a satellite feature at 64 eV and a main peak at 78 eV.[44,45] Following the results of band structure calculations, this double peak structure of the Si $L_{2,3}VV$ Auger transition in SiO_2 reflects the participation of Si valence states in two of the three valence band regions which are characteristic for the valence band of 4:2 coordinated silica polymorphs.[47,48] The satellite peak at 64 eV involves Si states weakly intermixing with the high binding energy, semicorelike O_{2s} valence band region V_1 and is termed the Si $L_{2,3}V_1V_2$ line. The main peak at 78 eV results from the strong participation of Si valence orbitals in the low binding energy, strongly bonding O_{2p}-$Si_{3s,3p}$ valence band region V_2 and is named the Si $L_{2,3}V_2V_2$ line. As the lowest binding energy valence band region V_3 in SiO_2 is an essentially nonbonding O_{2p} band, no Si states are involved and it remains thus undetected in the AES data.

Given the high photosensitivity of O_{2p} states with respect to the excitation by He I light,[49] He I UP spectra supplement the AES valence band data to study in particular the nonbonding O_{2p} silica valence band region V_3 of the silica layer on the Mo(112) surface (right panel in Fig. 6). The UP spectrum of the clean Mo(112) surface (0) is shown for comparison and is in line with the results of a recent angle-resolved photoelectron spectroscopy (ARPES) and inverse photoelectron spectroscopy (IPES) study in which the origin of the different peaks in the spectrum is discussed in detail.[50,51] The freshly deposited silica film changes the UP spectrum of the Mo(112) surface substantially. On the basis of He I UP studies of 4:2 coordinated silica modifications reported in the

literature,[52] the high binding energy valence band region from −10 to −12.5 eV can be attributed to the strongly bonding O_{2p}-$Si_{3s,3p}$ valence band region V_2 and the broad unstructured valence band region from −4.3 to −9 eV corresponds in width and structure to the nonbonding O_{2p} derived valence band region V_3. It is interesting to note that all He I UP spectra of amorphous silica samples show such a broad unstructured nonbonding valence band region V_3,[53,54] and it is only in the case of crystalline α-quartz samples that a two peak fine structure has been detected.[52,55] This two peak fine structure in the nonbonding O_{2p} valence band region V_3 is detected with unprecedented resolution in the He I UP valence band spectrum of the silica layer on the Mo(112) after application of the annealing procedure [spectrum (8)]. In addition, a third peak structure of unknown origin is found in the region V_3 and forms a small shoulder at −5.2 eV binding energy close to the upper silica valence band edge [arrow in spectrum (8)]. Clearly, this high resolution in the He I UP spectrum (8) can be attributed to the advantageous situation of studying an ultrathin well-ordered silica layer on a conducting metal substrate so that inhomogeneous broadening effects (sample charging, structural disorder, etc.) are minimized.

IV. DISCUSSION

The results of the presented surface science studies are used in the following to set up growth and structure models of the silica epilayer on the Mo(112) surface.

A. The growth model of the silica layer

Figure 7 summarizes the most important surface processes which play a key role in the growth of well-ordered silica films on the Mo(112) surface. During the silica film deposition two different preparation states can be distinguished (upper panel in Fig. 7). The *first state* of the silica film growth is marked by the deposition of silica on the Mo(112) surface [panels (1) and (2)]. The LEED and SPA-LEED studies detect a high tendency for the formation of an initially well-ordered silica layer which wets the substrate surface. Furthermore, the SPA-LEED clearly shows that the thin silica overlayer is split into a grid of misfit dislocations lines which run along both substrate directions (dashed lines in Fig. 7). As pointed out above, IRAS and XPS studies indicate that the properties of this initial silica layer differ from bulk silica samples. In addition, a previously reported TDS study has shown that the initial silica layer is not thick enough to completely suppress the interaction of the Mo(112) substrate with simple gases such as deuterium (D_2).[11] Aiming at the use the system SiO_2/Mo(112) as silica model oxide support in future catalyst studies, a thicker silica film must be grown. During the *second state* of the silica film growth, silica is mainly deposited on the initially formed silica layer [panel (3) and (4)]. Here, it has been shown in the previous discussion that LEED, SPA-LEED, and IRAS studies detect a roughening of the silica layer. As these rough silica surfaces turn out not to be stable against the high-temperature treatment of the silica film annealing

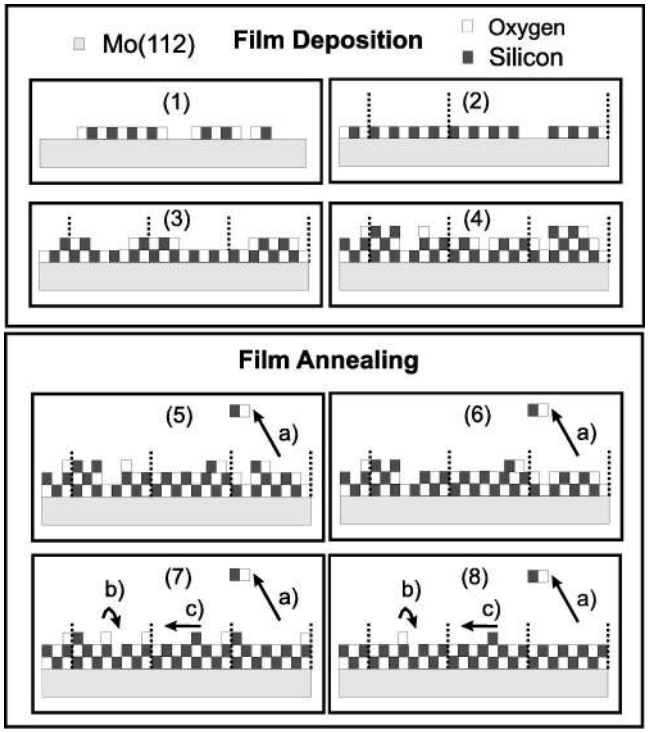

FIG. 7. Overview of the growth process of well-ordered silica epilayers on the Mo(112) surface during the silica film deposition (1–4) (*upper panel*) and during the silica film annealing procedure (5–8) (*bottom panel*) (see text).

procedure, the surface roughening is attributed to a kinetically limited growth region. The surface mobility of the silica deposits on silica is simply too low under the film deposition conditions to allow the epilayer to reach its thermodynamic equilibrium morphology.

To drive the silica epilayer to its thermodynamic equilibrium, the silica film is annealed to activate different surface processes (bottom panel in Fig. 7). As detected by XPS, the annealing procedure is accompanied by a minor loss of silica due to a partial reevaporation [process (a)]. However, more effective are the surface processes (b) and (c) during the annealing steps [panels (7) and (8)] which are revealed in the SPA-LEED and in particular in the STM studies. The transformation of the initially rough silica film into a silica epilayer structure with a flat surface reflects the spreading of 3D silica conglomerates over the silica surface [process (b)]. This spreading mechanism increases also the Si LVV auger electron signal, as detected by plotting the *a*uger electron *s*ignal versus annealing *t*ime (AS-*t* plot) in a quantitative AES study of the silica film growth.[14] Furthermore, the formation of a step structure in form of stripes during the annealing process by a decoration of the $[\bar{1}\bar{1}1]$ dislocation lines [process (c)] is found as an intermediate case. As both these processes (b) and (c) involve a directed material transport, it is not surprising that these mechanisms do not become important before annealing temperatures above 1150 K are applied. This is true because it is known that the viscous flow of the silica network starts in this temperature regime.[56,57] Certainly, the surface process (b) is of particular importance for the preparation of flat silica surfaces with a

homogeneous thickness because it results in the completion of early silica monolayers at the cost of higher film levels. These results suggest that a Frank–van der Merwe growth mode is thermodynamically favored in the studied thickness range of the silica epilayer.

B. The structure models of the silica layer

The silica epilayer structure models on the Mo(112) surface have been constructed with the help of a concept for heteroepitaxial systems first introduced by Bollmann *et al.*[58] Following this approach, low-index silica surfaces are attached to the Mo(112) substrate surface with such an azimuthal orientation that, if necessary at all, only a small lattice distortion is required to produce the maximum number of lattice coincidence points between the film and substrate lattice. Certainly, these silica epilayer structure models must be in line with the experimental results of the above discussed surface science studies. Therefore, only low-index silica surfaces of 4:2 *coordinated silica polymorphs* (AES/UPS valence band study) have been considered which can be *attached via oxygen atoms* (XPS study) to the Mo(112) surface and yield the observed *surface unit cell spacing* (LEED/STM study).

The Bollmann approach results in two independent silica epilayer structure models, namely, the HP-tridymite/β-cristobalite [panel (A) in Fig. 8] and the low/high quartz model [panel (B) in Fig. 8]. As explained in the following, these models are derived by considering hexagonal silica surface orientations of these silica polymorphs which require only a small lattice distortion in the attachment process to the Mo(112) surface to yield the $c(2\times2)$ silica epilayer structure.

The *bulk-determined hexagonal silica surface lattices of the silica polymorphs* are depicted in the graphs (A1) and (B1) of Fig. 8. Each graph contains four silica unit cells and one unit cell is indicated by dashed lines. Silicon atoms (big spheres) are sketched in the centers of the silica tetrahedra (triangular faces) which are interconnected via oxygen edge atoms (small spheres and asterisks). This reproduces the well-known network of corner sharing tetrahedra of the 4:2 coordinated silica polymorphs.[59] In case of the HP-tridymite/β-cristobalite model (A), the bulk lattices of HP-tridymite and β-cristobalite are polytypic, i.e., these two silica polymorphs result when the hexagonal fundamental module with a unit cell length of $b=5.05$ Å [depicted in panel (A1)] is stacked with a sequence *AB* along the [0001] direction (HP-tridymite) or a sequence *ABC* along the [111] direction (β-cristobalite). In the case of the low/high quartz model (B), the two quartz modifications are related by a displacive phase transition which involves a small, but simultaneous tilt of all silica tetrahedra.[59] Rather small changes in the atomic positions result so that the present discussion is limited to the hexagonal (0001) basal plane of low quartz with a unit cell length of $b=4.91$ Å [sketched in panel (B1)], but can be equally applied to the (0001) basal plane of high quartz.[14]

The $c(2\times2)$ *oxygen interface models of the silica epilayer structure models* are sketched in the bottom graphs (A2) and (B2) of Fig. 8. The attachment of the oxygen atoms of the above discussed silica surfaces in the potential adsorption sites on the trough (big white spheres) and row (big white gray spheres) Mo(112) structure introduces a small silica lattice distortion which reduces the hexagonal symmetry of the silica surfaces towards a $c(2\times2)$ surface unit mesh.

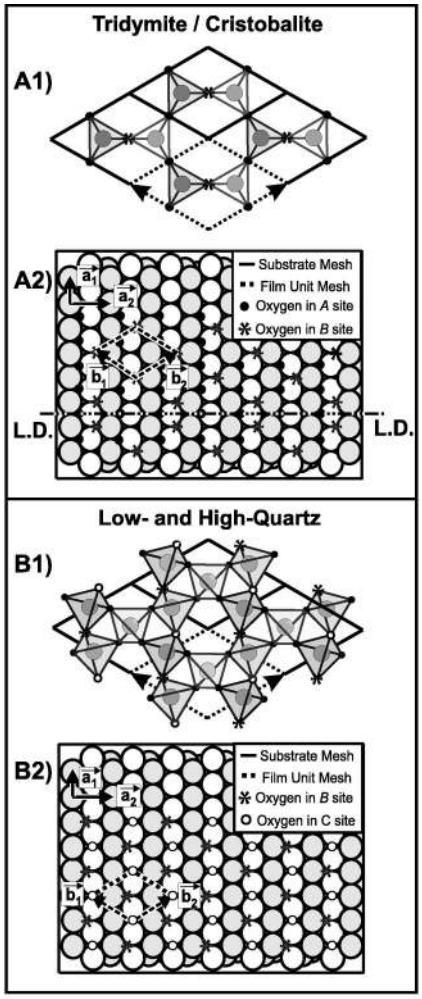

FIG. 8. The HP-tridymite/β-cristobalite (A) and the low/high quartz (B) silica epilayer structure models on the Mo(112) surface. The top panels (A1) and (B1) show the *bulk-determined hexagonal silica surfaces* of the respective silica polymorphs which are attached via oxygen atoms to the substrate. The resulting *oxygen interface structure models* of the silica epilayer on the Mo(112) substrate are shown in the corresponding bottom panels (A2) and (B2). The coordinate system a (b) indicates the substrate (film) unit mesh. A *l*ine *d*efect with $[\bar{1}10]$ orientation is sketched in the oxygen interface structure model (A2) (see text).

In case of the HP-tridymite/β-cristobalite model (A), silica tetrahedra are attached with their triangular faces to the Mo(112) surface. This is done by locating the oxygen atoms in the two sets of quasithreefold adsorption sites offered by the Mo(112) surface and denoted *A* (two row and one trough Mo atom) and *B* (one row and two trough atom) in Fig. 8. As the results of the effective medium theory suggest a higher tendency for oxygen adsorption to take place in the *A* sites, two of the three oxygen atoms of each silica tetrahedron face are attached to these sites.[60] These oxygen atoms are de-

picted in form of small filled circles in Fig. 8. This results in rows of oxygen atoms along the $[\bar{1}\bar{1}1]$ direction. The remaining third oxygen atom of each triangular silica tetrahedron face is adsorbed in a quasithreefold *B* site (asterisks in Fig. 8). With this procedure, an oxygen-oxygen spacing on the Mo(112) surface of 2.73 Å results which is only 4% larger than the corresponding oxygen-oxygen distance of 2.61 Å in the bulk silica polymorphs. After attaching in this way the interfacing plane of oxygen atoms to the Mo(112) surface, the bulk silica polymorphs structures can start to grow. Thus, it seems possible that a slight distortion of the fundamental stacking module enables the growth of well-ordered HP-tridymite layers with a (0001) orientation $[(112)_{\mathrm{Mo}}\|(0001)_{\text{HP-tridymite}}]$ or β-cristobalite films with a (111) orientation $[(11\bar{2})_{\mathrm{Mo}}\|(111)_{\beta\text{-cristobalite}}]$ on the Mo(112) substrate surface. In both cases, the HP-tridymite/β-cristobalite structure model produces a $c(2\times2)$ film unit mesh where the unit cell vectors span an angle of 63° and have a length of 5.22 Å (film coordinate system $\vec{b}$ in Fig. 8). These values correspond within 5% to the bulk unit cell dimensions of the hexagonal stacking module in HP-tridymite and β-cristobalite.

In the case of the low/high quartz model (B), silica tetrahedra are attached with their edges to the Mo(112) substrate surface. In the interface structure model (B2) in Fig. 8, it is seen that oxygen atoms marked by asterisks occupy quasithreefold hollow *B* sites and oxygen atoms depicted by small open circles are situated in twofold bridging positions *C* on the Mo(112) surface. Zigzag chains of oxygen atoms are formed in the troughs of the Mo(112) surface which run in the $[\bar{1}\bar{1}1]$ direction. The oxygen-oxygen distance between *B* and *C* sites on the Mo(112) surface is 2.73 Å so that it fits again within 4% to the bulk value of 2.61 Å in low quartz. After setting up the oxygen interface plane on the Mo(112) surface, the low quartz structure can start to grow with a [0001] orientation $[(112)_{\mathrm{Mo}}\|(0001)_{\text{low-quartz}}]$. It is seen that the pseudomorphic growth of low quartz on the Mo(112) surface produces the observed $c(2\times2)$ surface unit mesh with the film unit cell vectors spanning an angle of 63° and having a length of 5.22 Å (film coordinate system $\vec{b}$ in Fig. 8). The influence of the substrate results in an extension of the unit cell dimensions ($b=4.9124$ Å) of the bulk hexagonal (0001) low quartz surface structure by about 6%. Note that the attachment of the bulk hexagonal (0001) high quartz structure ($b=4.9977$ Å) to the Mo(112) surface in a very similar way requires an extension of the unit cell dimensions of just about 4%.

An interesting point concerns the construction of domain wall models for the line defects observed in the silica epilayer. Antiphase domain boundaries along the $[\bar{1}10]$ and $[\bar{1}\bar{1}1]$ direction result when two neighboring crystalline silica domains are displaced with respect to each other by a displacement vector $\vec{D}=\vec{a}_1$ and $\vec{a}_2$, respectively. As outlined elsewhere,[14] a stacking fault $\vec{D}=\vec{a}_2$ is not compatible with the discussed silica lattices so that a distorted domain wall morphology (broken bonds, disordered material, etc.) results for line defects with $[\bar{1}\bar{1}1]$ orientation. In contrast to this, misfit dislocation lines along the $[\bar{1}10]$ direction are compatible with the silica structures because a stacking fault $\vec{D}=\vec{a}_1$ between two neighboring domains yields only a minimial distortion of the lattices along the boundary. This situation is shown for the HP-tridymite/β-cristobalite model (A) in the panel (A2). The *l*ine *d*efect with $[\bar{1}10]$ orientation is marked by a dashed horizontal line labeled (LD) and separates two silica domains which are displaced with respect to each other by $\vec{D}=\vec{a}_1$. This displacement results from a corresponding stacking fault of the oxygen atoms in *B* sites (asterisks), but no interruption of the rows of oxygen atoms in *A* sites (small filled circles) results. In case of the low/high quartz model (B), line defects of this kind are well known as the Brazil boundaries along which the two enantiomorphs in low/high quartz crystals are twined.[14]

In conclusion, the here proposed silica epilayer structure models derive a qualitative understanding of the unit cell dimensions and the line defect structure of the silica layer on the Mo(112) surface. Any attempt to judge which of the proposed structure models is more suitable to account for the characteristics of the system SiO_2/Mo(112) requires new insights, either from experimental studies or theoretical calculations.

V. CONCLUSION AND OUTLOOK

Ultrathin well-ordered silica epilayers grown on a Mo(112) substrate mimic perfectly the electronic properties of bulk silica samples. Since their morphological properties (reproducible defect structure, low surface roughness) can be sufficiently controlled, the heteroepitaxial system SiO_2/Mo(112) can be used as a silica model oxide support in the field of model catalyst surface science studies. These studies aim to derive an atomic scale description of the important processes involved in the catalytic reactions. Two important preconditions are necessary to achieve this goal. First, the silica epilayer must cover the whole Mo(112) metal surface in order to exclude any influence of the Mo substrate on the chemistry of the catalytic reaction. The presented multitechnique surface science study sets up a growth model of the silica epilayer in which its continuous nature on the Mo(112) surface is confirmed by several methods. Secondly, the crystallographic structure of the silica layer must be solved. The surface science studies yield several pieces of crystallographic information which are successfully combined in first structure models. A surface x-ray *d*iffraction (SXD) experiment at the *E*uropean *s*ynchrotron *r*adiation *f*acility (ESRF) is currently under way to tackle the structure problem in detail.

ACKNOWLEDGMENTS

We are grateful to a number of agencies for financial support: Deutsche Forschungsgemeinschaft (DFG), Bundesministerium für Bildung und Forschung (BMBF), and Fonds der Chemischen Industrie. J.B.G. would like to thank the Alexander von Humboldt Foundation for financial support.

*Present Address: Department of Chemistry, University of Ottawa, 10 Marie Curie, Ottawa, ON, KIN 6N5, Canada. Electronic address: javier.giorgi@science.uottawa.ca

[1] M. Bäumer and H.-J. Freund, Prog. Surf. Sci. **61**, 127 (1999).
[2] C. R. Henry, Surf. Sci. Rep. **31**, 231 (1998).
[3] C. T. Campbell, Surf. Sci. Rep. **27**, 1 (1997).
[4] X. Xu and D. W. Goodman, Surf. Sci. **282**, 323 (1993).
[5] J.-W. He, X. Xu, J. S. Corneille, and D. W. Goodman, Surf. Sci. **279**, 119 (1992).
[6] X. Xu, S. M. Vesecky, and D. W. Goodman, Science **258**, 788 (1992).
[7] A. Kohl, S. Labich, E. Taglauer, and H. Knözinger, Surf. Sci. **454–456**, 974 (2000).
[8] J. T. Mayer, R. F. Lin, and E. Garfunkel, Surf. Sci. **265**, 102 (1992).
[9] J. W. Keister, J. E. Rowe, J. J. Kolodziej, and T. E. Madey, J. Vac. Sci. Technol. B **18**, 2174 (2000).
[10] T. Schroeder, M. Adelt, B. Richter, M. Naschitzki, M. Bäumer, and H.-J. Freund, Microelectron. Reliab. **40**, 841 (2000).
[11] T. Schroeder, M. Adelt, B. Richter, M. Naschitzki, M. Bäumer, and H.-J. Freund, Surf. Rev. Lett. **7**, 7 (2000).
[12] T. Schroeder, A. Hammoudeh, M. Pykavy, N. Magg, M. Adelt, M. Bäumer, and H.-J. Freund, Solid-State Electron. **45**, 1471 (2001).
[13] J. B. Giorgi, T. Schroeder, M. Bäumer, and H.-J. Freund, Surf. Sci. Lett. **498**, L71 (2002).
[14] T. Schroeder, Ph.D. thesis, Humboldt-Universität, Berlin, 2001.
[15] T. Schroeder, J. B. Giorgi, N. Magg, A. Hammoudeh, M. Bäumer, and H.-J. Freund, Phys. Rev. B **65**, 115411 (2002).
[16] A. J. C. Wilson, *X-Ray Optics*, 2nd ed. (Methuen, London, 1962).
[17] M. Horn-Von Hoegen, Z. Kristallogr. **214**, 1 (1999).
[18] C. S. Lent and P. I. Cohen, Surf. Sci. **139**, 121 (1984).
[19] P. R. Pukite, C. S. Lent, and P. I. Cohen, Surf. Sci. **161**, 39 (1985).
[20] H. Ikegami, K. Ohmori, H. Ikeda, H. Iwano, S. Zaima, and Y. Yasuda, Jpn. J. Appl. Phys. **35**, 1593 (1996).
[21] H. Watanabe, K. Fujita, and M. Ichikawa, Appl. Phys. Lett. **72**, 1987 (1998).
[22] D. A. Bonnell, Prog. Surf. Sci. **57**, 187 (1998).
[23] J. Wollschläger, J. Falta, and M. Henzler, Appl. Phys. A: Solids Surf. **50**, 57 (1990).
[24] U. Durig, O. Zuger, and D. W. Pohl, J. Microsc. **152**, 259 (1988).
[25] G. Ceballos, Z. Song, J. I. Pascual, H.-P. Rust, H. Conrad, M. Bäumer, and H.-J. Freund, Chem. Phys. Lett. **359**, 41 (2002).
[26] B. Harbecke, B. Heinz, and P. Grosse, Appl. Phys. A: Solids Surf. **38**, 263 (1985).
[27] P. Grosse, B. Harbecke, B. Heinz, and R. Meyer, Appl. Phys. A: Solids Surf. **39**, 257 (1986).
[28] D. W. Berreman, Phys. Rev. **130**, 2193 (1963).
[29] T. Sasaki, Y. Goto, R. Tero, K. Fukui, and Y. Iwasawa, Surf. Sci. **502–503**, 136 (2002).
[30] A. Pasquarello and R. Car, Phys. Rev. Lett. **79**, 1766 (1997).
[31] J. Sarntheim, A. Pasquarello, and R. Car, Science **275**, 1925 (1997).
[32] B. A. Morrow and A. J. McFarlan, J. Phys. Chem. **96**, 1395 (1992).
[33] E. Dowty, Phys. Chem. Miner. **14**, 80 (1987).
[34] A. M. Hofmeister, J. Xu, and S. Akimoto, Am. Mineral. **75**, 951 (1990).
[35] J. Etchepare, M. Merian, and I. Smetankine, J. Chem. Phys. **60**, 1873 (1974).
[36] J. Etchepare, M. Merian, and P. Kaplan, J. Chem. Phys. **68**, 1531 (1978).
[37] N. Arul Dhas and A. Gedanken, J. Phys. Chem. **101**, 9495 (1997).
[38] F. M. Hoffmann, Surf. Sci. Rep. **3**, 107 (1983).
[39] P. Lange, J. Appl. Phys. **66**, 201 (1989).
[40] C. T. Kirk, Phys. Rev. B **38**, 1255 (1988).
[41] A. C. Diebold, D. Venables, Y. Chabal, D. Muller, M. Weldon, and E. Garfunkel, Mater. Sci. Semicond. Process. **2**, 103 (1999).
[42] M. L. Colaianni, J. G. Chen, W. H. Weinberg, and J. T. Yates, Jr., Surf. Sci. **279**, 211 (1992).
[43] C. Zhang and G. A. Somorjai, Surf. Sci. **149**, 326 (1984).
[44] B. Carriere and B. Lang, Surf. Sci. **64**, 209 (1977).
[45] B. Carriere and J. P. Deville, Surf. Sci. **80**, 278 (1979).
[46] A. Hiraki, Surf. Sci. Rep. **3**, 357 (1984).
[47] J. R. Chelikowsky and M. Schlüter, Phys. Rev. B **15**, 4020 (1977).
[48] D. L. Griscom, J. Non-Cryst. Solids **24**, 155 (1977).
[49] J. J. Yeh and I. Lindau, At. Data Nucl. Data Tables **32**, 1 (1985).
[50] T. McAvoy, J. Zhang, C. Waldfried, D. N. McIlroy, P. A. Dowben, O. Zeybeck, T. Bertrams, and S. D. Barrett, Eur. Phys. J. B **14**, 747 (2000).
[51] I. N. Yakovkin, J. Zhang, and P. A. Dowben, Phys. Rev. B **63**, 115408 (2001).
[52] A. Di Pomponio, A. Continenza, L. Lozzi, M. Passacantando, S. Santucci, and P. Picozzi, Solid State Commun. **95**, 313 (1995).
[53] H. Ibach and J. E. Rowe, Phys. Rev. B **10**, 710 (1974).
[54] F. G. Bell and L. Ley, Phys. Rev. B **37**, 8383 (1988).
[55] T. H. DiStefano and D. E. Eastman, Phys. Rev. Lett. **27**, 1560 (1971).
[56] C. L. Claeys, R. F. de Keersmaecker, and G. J. Declerck, in *The Silicon-Silica System*, edited by P. Balk (Elsevier, Amsterdam, 1988), Chap. 4.
[57] S. Miyazaki, H. Nishimura, M. Fukuda, L. Ley, and J. Ristein, Appl. Surf. Sci. **113/114**, 585 (1997).
[58] W. Bollmann, Philos. Mag. **16**, 363 (1967).
[59] P. J. Heaney, Rev. Mineral. **29**, 1 (1994).
[60] J. K. Norskov and N. D. Lang, Phys. Rev. B **21**, 3037 (1980).